The current issue and full text archive of this journal is available at
www.emeraldinsight.com/0961-5539.htm

An evaluation of synthetic jets for heat transfer enhancement in air cooled micro-channels

Victoria Timchenko, John Reizes and Eddie Leonardi
School of Mechanical & Manufacturing Engineering, The University of NSW, Sydney, Australia

Received 1 January 2006
Accepted 9 July 2006

Abstract

Purpose – The development of novel cooling techniques is needed in order to be able to substantially increase the performance of integrated electronic circuits whose operations are limited by the maximum allowable temperature. Air cooled micro-channels etched in the silicon substrate have the potential to remove heat directly from the chip. For reasonable pressure drops, the flow in micro-channels is inherently laminar, so that the heat transfer is not very large. A synthetic jet may be used to improve mixing, thereby considerably increasing heat transfer. This paper seeks to address this issue.

Design/methodology/approach – CFD has been used to study the flow and thermal fields in forced convection in a two-dimensional micro-channel with an inbuilt synthetic jet actuator. The unsteady Navier-Stokes and energy equations are solved. The effects of variation of the frequency of the jet at a fixed pressure difference between the ends of the channel and with a fixed jet Reynolds number, have been studied with air as the working fluid. Although the velocities are very low, the compressibility of air has to be taken into account.

Findings – The use of a synthetic jet appreciably increases the rate of heat transfer. However, in the frequency range studied, whilst there are significant changes in the details of the flow, due primarily to large phase changes with frequency, there is little effect of the frequency on the overall rate heat transfer. The rates of heat transfer are not sufficiently large for air to be a useful cooling medium for the anticipated very large heat transfer rates in future generations of microchips.

Research limitations/implications – The study is limited to two-dimensional flows so that the effect of other walls is not considered.

Practical implications – It does not seem likely that air flowing in channels etched in the substrate of integrated circuits can be successfully used to cool future, much more powerful microchips, despite a significant increase in the heat transfer caused by synthetic jet actuators.

Originality/value – CFD is used to determine the thermal performance of air flowing in micro-channels with and without synthetic jet actuators as a means of cooling microchips. It has been demonstrated that synthetic jets significantly increase the rate of heat transfer in the micro-channel, but that changing the frequency with the same resulting jet Reynolds number does not have an effect on the overall rate of heat transfer. The significant effect of compressibility on the phase shifts and more importantly on the apparently anomalous heat transfer from the "cold" air to the "hot" wall is also demonstrated.

Keywords Heat transfer, Fluid dynamics, Jets, Simulation

Paper type Technical paper

The authors wish to thank the Australian Research Council for providing financial support for this work.

International Journal of Numerical Methods for Heat & Fluid Flow
Vol. 17 No. 3, 2007
pp. 263-283

0961-5539
DOI 10.1108/09615530710730148

Introduction

Since, one of the performance limiting factors of microchips is the maximum allowable temperature, and since it appears that the presently available temperature control methods will not be adequate in future microchip technology, the development of novel cooling techniques is necessary in order to sustain the rate of development of integrated electronic circuits. Forced air convection in micro-channels etched in the silicon substrate has the potential to remove heat directly from the chip and has been used as one of the strategies for cooling integrated circuits (Tuckerman and Pease, 1981). Since, for reasonable pressure drops across the channel, the flow in micro-channels is inherently laminar and the heat transfer is not, in fact, very large. In addition, if the upper surfaces of the micro-channels are hot, the heat transfer on that surface may be further reduced by separations near the inlet. Some method of providing better mixing is therefore, necessary in order to increase the rate of heat transfer.

It is proposed to use synthetic jets to "disrupt" the laminar flow in the channels thereby creating better mixing with the mean flow, whilst at the same time interfering with the stagnant zones. A synthetic jet (Glezer and Amitay, 2002) can be developed in the cooling fluid by a micro-pump actuator (Mallinson *et al.*, 2003). This consists of an oscillating membrane in a cavity with a small orifice in the face opposite the diaphragm. When "steady conditions" on the average over a cycle have been reached, the actuator has a zero net mass flow through the orifice, but a non-zero net momentum transfer over an entire period of the diaphragm oscillation. Under appropriate operating conditions this actuator provides a fluctuating flow away from the orifice into the cooling channel, thereby creating a "quasi-turbulent" flow. As a result, it may be possible to significantly increase the rate of heat transfer when this jet impinges on a hot surface. This process is quite different to that which is obtained when the synthetic jet is discharged into a quiescent atmosphere (Timchenko *et al.*, 2004).

An experimental study of periodic disturbances on the penetration and mixing of synthetic jets in cross-flow was performed by Eroglu and Breidenthal (2001). They observed that periodic forcing of the jet stream affects mixing by creating vortex loops whose strength and spacing are determined by the frequency of the forcing jet and the jet-to-cross-flow velocity ratio. The main parameter characterizing the jet in cross-flow was found to be the jet-to-cross-flow momentum ratio. The effect of periodic disturbances on the coherent flow structures and heat transfer in the case of an impinging air jet was studied experimentally by Mladin and Zumbrunnen (2000). Their results suggest that the large coherent flow structures associated with a high amplitude, high frequency flow pulses increase the Nusselt number at the stagnation line by surface renewal effects. Similar effects had been previously demonstrated by Kataoka *et al.* (1987) for steady impinging flows. The most significant effect on the enhancement of heat transfer corresponded to high values of the product $St\ A_N$ in which St is the Strouhal number and A_N is the ratio of the amplitude of the velocity pulsation to the time-averaged velocity at the jet nozzle exit. Their results for a free (non-impinging) jet agreed with those of Ho and Huang (1982) who had demonstrated that in the presence of an external periodic disturbance, large flow structures have their frequency fixed by the forcing disturbance. They also showed that the large structures, formed within the mixing layers at $1/f$ time intervals travel with a constant velocity. Since, the frequency of the large structures matched the forcing frequency, f, it follows that their wavelength and size decreased with forcing frequency.

All previous studies of periodic disturbances and their effect on heat transfer have been performed on macro-scale turbulent flows. In this work we intend to introduce the same sort of disturbances using synthetic jets, in laminar flows, in micro-sized devices. We study numerically the behaviour of a synthetic jet in cross-flow constrained in a micro-channel with a hot top wall and determine its effect on the distribution of heat flux. Computations of unsteady compressible laminar flow are performed for the two-dimensional channel including the fluid motion and temperature variations within the synthetic jet actuator cavity. The amplitude of membrane deflection was varied at different frequencies so as to maintain an approximately constant the average velocity at the exit the orifice. The effectiveness of the proposed technique for cooling microchips is evaluated by comparing the heat transfer rates when the synthetic jet is operating, with those obtained when the synthetic jet is not used and with each other at different frequencies.

Mathematical and numerical model

A two-dimensional micro-channel 200 μm high and 4.2 mm long has been used. It is open at either end with the top surface hot and all the other walls adiabatic. Parts of the regions outside the channel have been included in the calculations as may be seen in Figure 1.

For micro-sized devices the flow is dependent on the Knudsen number, Kn, which is the ratio of the mean free path of the gas molecules to a characteristic length, for example, $Kn = \lambda/d$ in the orifice. Since, in this study flows with $Kn < 0.01$ have been modelled, the continuum approach using conventional conservation equations is valid (Karniadakis and Beskok, 2002). The transient compressible flows generated by the constant 250 Pa pressure difference between the ends of the channel and by the synthetic jet actuator have been simulated using a commercial package, CFX-5.7.

The set of the unsteady conservation equations for laminar flow comprises the continuity equation:

$$\frac{\partial \rho}{\partial t} + \nabla(\rho \tilde{V}) = 0, \tag{1}$$

the Navier-Stokes equation:

$$\frac{\partial \rho \tilde{V}}{\partial t} + \nabla(\rho \tilde{V}\tilde{V}) = -\nabla p + \nabla(\mu(\nabla \tilde{V} + (\nabla \tilde{V})^T)) + \rho \tilde{g} \tag{2}$$

and the energy equation:

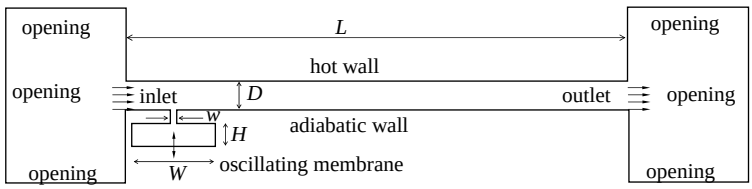

Figure 1.
Schematic diagram of channel and actuator

$$\frac{\partial \rho h_a}{\partial t} + \nabla(\rho \tilde{V} h_a) - \nabla(\lambda \nabla T) = 0, \tag{3}$$

in which, ρ, $\tilde{V}$, p, μ, h_a, T, λ, and t denote the density, the velocity vector, the gauge pressure, the dynamic viscosity, the specific enthalpy, the absolute temperature, the thermal conductivity and time, respectively. The compressibility of the air is taken into account by treating it as an ideal gas with:

$$\rho = \frac{(p + p_{\text{ref}})}{RT}, \tag{4}$$

in which R is the specific gas constant and p_{ref} is the absolute ambient pressure.

The displacement of the membrane Y_m was assumed to be a parabola, which varies sinusoidally in time, viz.:

$$Y_m = A\left(1 - \left(\frac{2x}{W}\right)^2\right)\sin(2\pi ft) \tag{5}$$

in which A is the centreline amplitude, f is the frequency of oscillation, respectively, and W is the width of the diaphragm (Figure 1). To simulate the displacement of the membrane an actual mesh deformation in the vicinity of the membrane has been applied accordingly to equation (5), so that computational domain has been reconstructed at each time step.

A second order backward Euler differencing scheme was used for the transient term, whereas a central differencing scheme was employed for the advection terms in the Navier Stokes equation. At each time step of a cycle, equal to one hundredth of the period of a cycle, the internal iterations were continued until the mass and momentum residuals had been reduced to 10^{-6}.

Validation of mathematical and numerical model has been performed in our earlier paper (Timchenko *et al.*, 2004) for the case of an incompressible synthetic jet in an axisymmetric configuration. Computed instantaneous stream-wise and transverse velocity profiles across the orifice exit were in very good agreement with numerical results (Mallinson *et al.*, 2003) validated against experimental data.

In general, when one refers to compressible flows it is understood that flows of Mach number greater than about 0.3 are to be discussed. However, in our case, even for the flow with Mach number much lower then 0.3 ($Ma = 4.5 \times 10^{-2}$), pressure and temperature differences lead to sufficiently large density changes which result in resonance effects thereby affecting the heat transfer results. It follows that an estimate of the natural frequency and the phase shifts to be expected is required, before evaluating the operation of synthetic jet actuators in micro channels in which air is used as the cooling fluid.

Natural frequency and phase shift in the cavity and orifice of the actuator

The determination of the natural frequency is derived from a linearised lumped parameter model of the cavity and the orifice. Typical flow within the cavity and the orifice obtained in this study at all frequencies are shown in Figure 2.

It appears that a column of air stretching from the lower edge of the main channel to the diaphragm with a width approximately equal to the width of the orifice, moves as

an oscillating body. Suppose therefore, that the column of air marked as ABCDEFGH in Figure 3, is moved down by a small distance Y from its equilibrium position, the mass m moved by the process is:

$$m = \rho(wb)(H + h), \tag{6}$$

in which the geometric variables w, b, h and H are shown in Figures 1 and 3.

It follows that the force, F_i, required to accelerate this mass is given by:

$$F_i = \rho(wb)(H + h)\frac{\mathrm{d}^2 Y}{\mathrm{d}t^2}. \tag{7}$$

If the pressure outside and inside the cavity are initially the same, the restoring force is provided by the pressure difference, Δp, between the cavity and the outside air in the main channel. Let the instantaneous pressure in the cavity be p_c and the pressure in the main channel at the orifice be p so that:

$$\Delta p = p_c - p. \tag{8}$$

If p is assumed to remain constant, the driving pressure is dependent only on p_c which can be determined if state path law is known. Assume that the expansion and compression processes in the cavity are isentropic, the state path law may be written:

$$p_c V_{ol}^{\gamma} = C, \tag{9}$$

in which, V_{ol} is the volume of the cavity excluding the oscillating column, γ is the ratio of the specific heat capacities and C is a constant. It follows from equation (9) that:

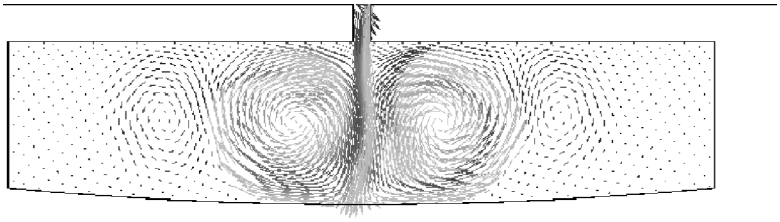

Figure 2.
Example of flow in the cavity and orifice passage at 10 kHz at the lowest position of the membrane

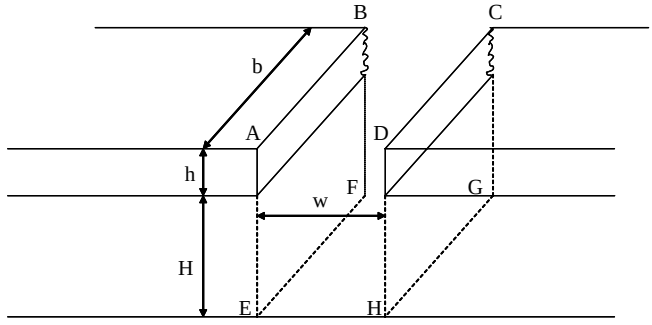

Figure 3.
Schematic diagram of air column in the cavity

$$\frac{\delta p_c}{p_c} + \gamma \frac{\delta V_{ol}}{V_{ol}} = 0, \tag{10}$$

in which δ indicates a small change.

Now, since $\delta V_{ol} = Ywb$ and $V_{ol} = (W - w)Hb$, δp_c can be evaluated from equation (10) as:

$$\delta p_c = -\frac{\gamma p_c w}{(W - w)H} Y. \tag{11}$$

The restoring force, F_r, is therefore given by:

$$F_r = \delta p_c wb = \frac{\gamma p_c w^2 b}{(W - w)H} Y. \tag{12}$$

All that remains is to determine the damping force, F_d, which consists of forces required to overcome friction in the orifice conduit and to generate and maintain the fluid motion in the cavity. The lowest estimate for F_d would therefore be the force required to overcome friction in the orifice passage. Because of the complex flows which occur in the orifice, it is not easy to obtain an estimate of the instantaneous losses in the orifice, so that the minimum possible approximation of F_d would be the steady state frictional force at the same instantaneous velocity, viz.:

$$F_d = \frac{12\mu bh}{w} \frac{dY}{dt}, \tag{13}$$

in which dY/dt represents the average velocity through the orifice.

The equation describing the motion of the air column can then be written as:

$$F_i + F_d + F_r = F_e \tag{14}$$

in which F_e is the external exciting force, in this case the force generated by the diaphragm and which can be written as:

$$F_e = K(f)b(2\pi f)^2 \sin(2\pi ft) \tag{15}$$

in which $K(f)$ is a constant related to the amplitude of the diaphragm motion in a complex way and is a function of the frequency f.

The substitution of equations (7), (12), (13) and (15) in equation (14) for F_i, F_r, F_d and F_e, respectively, leads to:

$$\rho(wb)(H + h)\frac{d^2Y}{dt^2} + \frac{12\mu bh}{w} \frac{dY}{dt} + \frac{\gamma p w^2 b}{(W - w)H} Y = K(f)b(2\pi f)^2 \sin(2\pi ft). \tag{16}$$

Since, the rate of change of the flow rate in the main channel is proportional to the frequency (Eroglu and Breidenthal, 2001), as the frequency becomes larger the accelerations and hence the pressure gradients in the main channel need to increase in the same way. This means that the amplitude of the pressure variations in the main channel will rise with the frequency. It follows that whilst $K(f)$ can be assumed to be a constant at a particular frequency of the diaphragm, it will vary as that frequency is changed and that is the main reason for writing $K(f)$ as a function.

Equation (16) can be simplified to:

$$\frac{d^2Y}{dt^2} + 2k\frac{dY}{dt} + (2\pi f_n)^2 Y = K_1(2\pi f)^2 \sin(2\pi ft) \tag{17}$$

in which:

$$k = \frac{(6\mu h)}{(\rho w^2(H+h))}, \tag{18}$$

$$f_n = \frac{1}{2\pi}\sqrt{\frac{(\gamma p w)}{(\rho(W-w)H(H+h))}} \tag{19}$$

is the natural frequency, which when employing the equation of state for the perfect gas becomes:

$$f_n = \frac{1}{2\pi}\sqrt{\frac{(\gamma R T_c w)}{((W-w)H(H+h))}} \tag{20}$$

and:

$$K_1(f) = \frac{K(f)}{(\rho w(H+h))} \tag{21}$$

The general solution to equation (21) (Kreyszig, 1972) is:

$$\begin{aligned} Y = {} & e^{-kt}(A\sin(2\pi ft) + B\cos(2\pi ft)) \\ & + \frac{K_1(f)(2\pi f)^2}{\sqrt{((2\pi f)^2 - (2\pi f_n)^2)^2 + 4k^2(2\pi f)^2}}\sin(2\pi ft - \beta), \end{aligned} \tag{22}$$

in which A and B are constants and the phase angle β is given by:

$$\beta = \tan^{-1}\left(\frac{4\pi kf}{(2\pi f_n)^2 - (2\pi f)^2}\right). \tag{23}$$

Once the initial transient has passed, equation (23) reduces to:

$$Y = \frac{K_1(f)(2\pi f)^2}{\sqrt{((2\pi f)^2 - (2\pi f_n)^2)^2 + 4k^2(2\pi f)^2}}\sin(2\pi ft - \beta) \tag{24}$$

so that the analytically average velocity at the exit of the orifice, $\bar{v}_O$ can be obtained by differentiation, viz.:

$$\bar{v}_O = \frac{K_1(f)(2\pi f)^3}{\sqrt{((2\pi f)^2 - (2\pi f_n)^2)^2 + 4k^2(2\pi f)^2}}\cos(2\pi ft - \beta). \tag{25}$$

Now the velocity of the diaphragm, v_m, is obtained by differentiating equation (5) yielding:

$$v_{\mathrm{m}} = A\left(1 - \left(\frac{2x}{W}\right)^2\right)(2\pi f)\cos(2\pi f t). \tag{26}$$

It may be seen by comparing equations (25) and (26) that β is the phase angle between the velocity of the diaphragm and the velocity through the orifice and that the orifice velocity lags the velocity at the diaphragm by an angle β.

Thus, it is now possible to evaluate the natural frequency and phase angle variations and discuss numerical results.

Results and discussion

To study the abilities of the synthetic jet to disrupt laminar flows in micro channels, an orifice 50 μm wide and 100 μm long was placed 1.2 mm downstream from the inlet. The width of the diaphragm was 2 mm and the cavity depth was 400 μm. Since, the inflow temperature and velocity distributions affect the heat transfer in the channel, external domains 1 mm long and 1.5 mm high were included at either end of the channel (Figure 1). A 250 Pa pressure was imposed at the inlet of the left external domain with the temperature set to 20°C. At the outlet, the right external domain, the pressure was programmed at zero, p_{ref} fixed at 100 kPa and the temperature set to 30°C. The upper wall of the channel was isothermal at 50°C. Grid points 50 × 20 in the stream-wise and transverse directions, respectively, were used in the orifice of the synthetic jet generator, so mesh size was kept to 2.5 μm in the orifice. Outside the orifice the grid was gradually expanded with a maximum mesh size equal to 5 μm. The total number of mesh points was equal to 164,316.

To describe the behaviour of pulsed jets in cross-flow, Eroglu and Breidenthal (2001) used a mean jet-to-cross-flow velocity ratio. Gordon and Soria (2001) characterized the jet in the cross-flow by the jet-to-cross-flow momentum ratio. Following Smith and Glezer (1998) we define the computed average velocity, $\bar{V}_j$ through the orifice only over the discharge period of the cycle, that is:

$$\bar{V}_j = \frac{2}{\tau w}\int_{t_0}^{t_0+\tau/2} \mathrm{d}t \int_{-w/2}^{w/2} V_j \,\mathrm{d}x \tag{27}$$

in which, t_0 is the time of beginning of discharge from the orifice, $\tau = 1/f$, is the period of diaphragm oscillation and V_j is the velocity at a point in the exit of orifice passage. Thus, the jet Reynolds number, Re_j, and the jet-to-cross-flow momentum ratio C_j, can be defined as $Re_j = \bar{V}_j w/\nu$ and:

$$C_j = \frac{\displaystyle\int_{-w/2}^{w/2}\int_{t_0}^{t_0+\tau/2} \rho V_j^2(x,t)\mathrm{d}x\,\mathrm{d}t}{\displaystyle\int_0^D \int_0^\tau \rho U_{\mathrm{ch}}^2(y,t)\mathrm{d}y\,\mathrm{d}t} \tag{28}$$

In this work the jet-to-cross-flow momentum ratio, $C_j \approx 8$ has been chosen as preliminary tests with the synthetic jet operating at $C_j < 8$ indicated that there was little effect on the heat transfer rate. Indeed, under these conditions the synthetic jet hardly reached the hot wall at all. As a consequence, an average jet velocity approximately 42 ms^{-1} was employed.

Steady flow results

The effectiveness of the proposed cooling strategy was evaluated by comparing the heat transfer effectiveness when the synthetic jet was operating with that obtained with the jet switched off. Temperature and vorticity contours with the jet not active may be seen in Figure 4.

The imposed pressures yielded an average velocity in the channel of $7.75\,\mathrm{ms}^{-1}$, that is a Reynolds number defined as $Re_{ch} = \bar{U}_{ch}D/\nu$ was equal to 103. The horizontal contours of vorticity indicate a laminar, parabolic flow with no mixing. This is confirmed by the velocity distributions shown in Figure 5(a).

The flow enters main channel with almost top hat distribution which gradually develops to a fully developed laminar flow. The lack of mixing is also illustrated in the steady flow temperature distribution shown in Figure 5(b). The temperature in the lower half of the channel has increased by less then 15 K whereas the potential temperature rise is 30 K which points to the fact that it should be possible to significantly increase them average heat transfer flux of $7.3\,\mathrm{kWm}^{-2}$ from the hot upper wall.

In order to evaluate the frequencies to be used in determining the effectiveness of introducing the synthetic jet to enhance the heat transfer rate, the natural frequency needs to be determined.

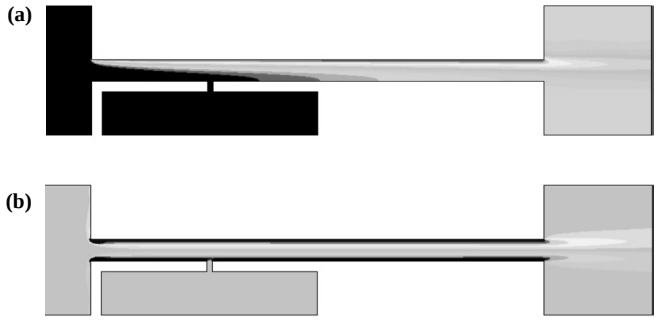

Figure 4.
(a) Temperature, $20°C \leq T \leq 50°C$; (b) vorticity, maximum positive $10^5\ s^{-1}$, minimum negative $-10^5\ s^{-1}$. Steady flow

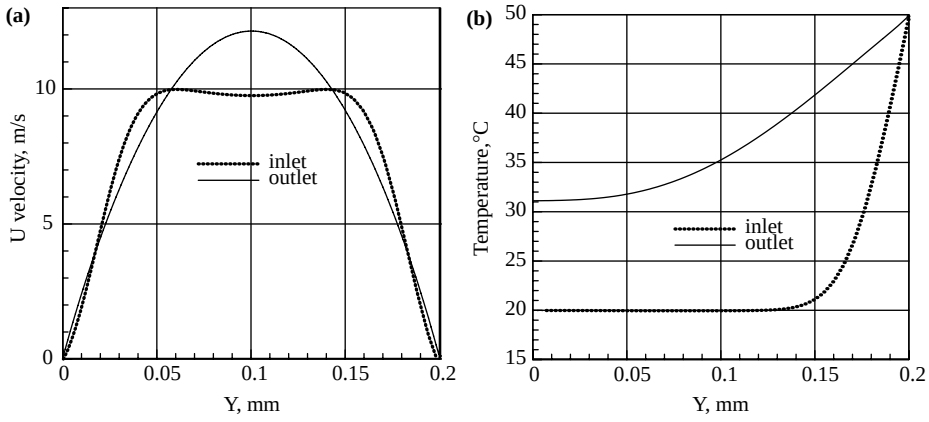

Figure 5.
(a) Horizontal velocity and (b) temperature profiles at the inlet and outlet of channel. Steady flow

Natural frequency and phase angle calculations

With $T_c \approx 300\,K$ and geometric parameters given above f_n was calculated from equation (19) as 19.88 kHz. Given the accuracy of the estimate, it may be assumed that $f_n = 20\,kHz$ with velocity at the orifice (equation (25)) lagging of velocity of the diaphragm (equation 25) by 90°. This is exactly the situation shown in Figure 6(a), in which at a diaphragm frequency of 20 kHz, the numerical results for the vertical velocity at the centre point of the exit of the orifice, lag the diaphragm velocity at the centre point by 90°. In Figure 6 time is normalised by the period of oscillation τ. Thus, the above simple theory is surprisingly accurate at predicting the natural frequency.

Since, the true transients have to be calculated that is small time steps had to be used, the run times were large, in the order of weeks, despite the significant computer resources deployed for the calculations. It follows that only two other frequencies were used, namely 10 and 30 kHz, one above and one below the natural frequency. Because of the phase shifts, valid comparisons between heat transfer distributions at various frequencies can only be performed if they are at the same point in cycle of the air motion at the orifice and not at the same point in the cycle as indicated by the motion of the diaphragm. It follows that it was necessary to determine the phase shift at each of the frequencies. Note, that amplitudes of oscillation were adjusted to keep the average jet velocity approximately the same and equal to $42\,ms^{-1}$.

The damping factor k did not have to be determined to evaluate the phase angle at a frequency of 20 kHz, because the denominator in equation (23) becomes zero at resonance, however in order to estimate β at 10 and 30 kHz, k needs to be evaluated. From equation (18), $k = 7.34 \times 10^3\,s^{-1}$. When this value is substituted into equation (18), $\beta \approx 4.5°$ results at a frequency of 10 kHz, whereas $\beta \approx 37°$ was obtained from the numerical experiments as may be seen in Figure 6(b). This difference was expected because of the underestimate of k discussed above in the development of the theory.

Now, a more appropriate estimate of the value of k may be obtained by using the actual value of β at 10 kHz, namely$\beta \approx 37°$ which leads to a value of $k = 7.1 \times 10^4\,s^{-1}$, nearly 10 times the value obtained from equation (18). The fluid motion in the cavity is generated and sustained by the movement the column of air (Figure 2). This process extracts energy from the air column. Further, the very complex flow in the orifice passage (Figure 2) leads to very significant "losses" not taken into account in equation (18). It is therefore not surprising that the actual value of k is very much larger than the initial estimate based on steady flow pressure losses. When the larger value of k is used in equation (23) to estimate the phase angle at 30 kHz, $\beta \approx 126°$ results. This value is remarkably close to $\beta \approx 124°$, the angle obtained in the CFD calculations as may be seen in Figure 6(c). Now that the phase changes are known, it is possible to discuss the details of the flow and the thermal fields and their effects on the heat transfer in main channel.

Fluid flow details

The computed instantaneous velocity vectors are shown in Figure 7 at different instants in the fourth cycle from the beginning of motion of the membrane when the diaphragm is operated at a frequency of 10 kHz. The structure of events remains approximately the same at all frequencies; the most significant change being the phase lag discussed above caused by compressibility effects in the cavity.

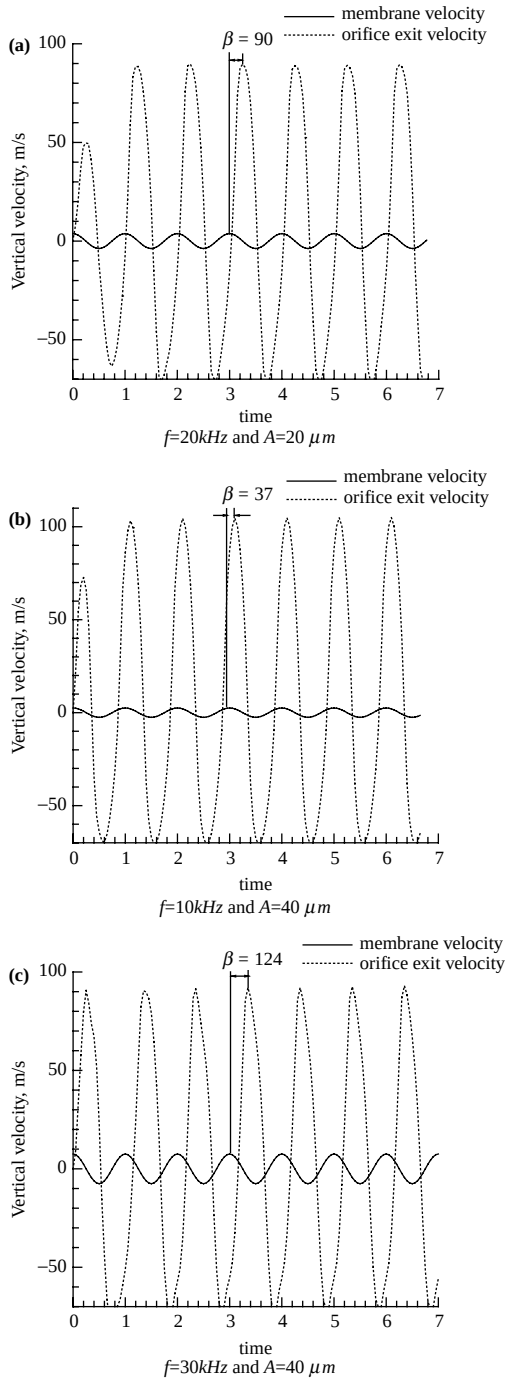

Figure 6.
Vertical velocity at centre point of membrane and centre point of exit of orifice

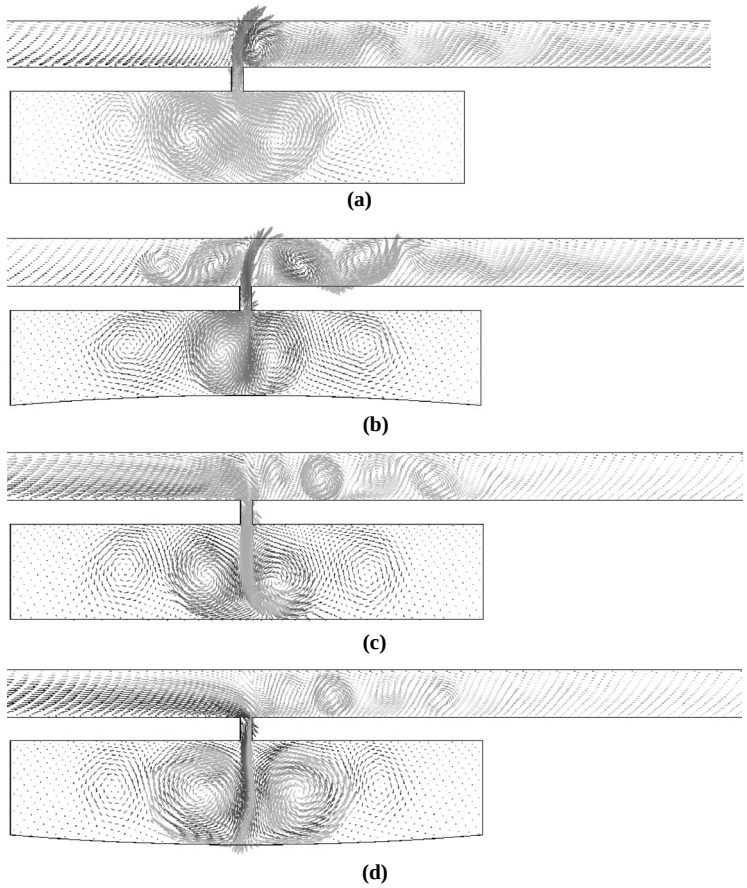

Figure 7.
Velocity vectors (a) $t = 3.0$; (b) $t = 3.25$; (c) $t = 3.5$; (d) $t = 3.75$ for $f = 10$ kHz and $A = 40\ \mu$m

The velocity vectors in Figure 7(a), occur at a time $t = 3.0$, when the diaphragm is moving at its maximum velocity towards the orifice. By this stage the expelled air from the orifice has reached the upper wall of the channel thereby interfering with the boundary layer in the region in which heat transfer occurs. The emerging jet from the orifice generated the clockwise vortex immediately down stream of the jet and at the same time it generated a small anticlockwise near the upper surface on the downstream side of the jet.

Since, the flow is two-dimensional, as may be seen in Figure 7(a), when the jet impinges on the upper surface the flow in the main channel is separated into two parts with no flow from the region upstream of the dividing jet to that down stream. This leads to a complete flow reversal in the area upstream of the jet so that a complex flow pattern begins to develop, caused by the interaction of the flow reversal and the developing vortex. Downstream of the impinging jet the motion is sustained by the jet and the remnant of the vortices from the previous cycle.

As may be seen in Figure 7(b), the impinging jet is reflected from the upper surface thereby strengthening the clockwise vortex generated when the jet emerging from the orifice on the downstream side of the orifice and forming a counter-clockwise vortex on

the downstream side of the first reflection from the upper wall. This new, counter clockwise vortex is strengthened by the reflection of the jet from the lower side. This is repeated a number of times so that a series of geared vortices are created which are separated by the main flow from the jet.

During the suction stage the geared vortices persist but weaken as time progresses while the axial velocity is reduced, as may be seen in Figure 7(c) and (d). What is not clear in Figure 7(c) that the vortex which was upstream of the orifice in Figure 7(b) has moved to be just downstream of the orifice. Similarly, the other vortices, shown in Figure 7(b) have moved downstream with significant loss of strength. The vortices continue to move downstream during the remainder of the suction phase as may be seen in Figure 7(d).

Further, during the suction phase, as may be seen in Figure 7(c) and (d) most of the fluid enters the cavity rather than continuing along the main channel, so that there is a significantly reduction in velocity in the main channel during the suction phase of the actuator cycle. It follows, that the velocity in the main channel, averaged over a cycle, is significantly reduced, in this case to $6.3\,\mathrm{ms}^{-1}$, from its steady flow value of $7.75\,\mathrm{ms}^{-1}$.

It is interesting to note that the structure of the synthetic jet in a confined cross-flow is completely different to that found in synthetic jets in still atmosphere. Synthetic jets in still atmosphere may appear to be continuous, vortices are generated at the orifice and travel in a direction parallel to the jet weakening as they move away from the orifice (Timchenko *et al.*, 2004). Under the same circumstances it is shown here that in a constrained cross flow the synthetic jet is not continuous. Moreover, whilst the vortices are convected in the direction of the main flow, they are generated both upstream and downstream of the orifice as well as by the reflections of the jet from the solid boundaries.

When the frequency of the diaphragm is increased to 20 and 30 kHz with the exit velocity from the orifice maintained at approximately the same value, the structure of the flow and the vortices at the same phase of the cycle relative to the jet velocity at the exit of the orifice passage, remains the same and need not be discussed any further.

When a quasi equilibrium condition is reached, the mass flow rate into the channel must be exactly equal that leaving the channel averaged over a cycle, so that the synthetic jet actuator becomes a zero net mass flow device, but in all the cases here this condition was not reached. The mass flow rate averaged over a cycle was always higher than the mass flow rate into the channel, indicating that the air in the cavity was warming up. Even after six cycles, the difference between the outflow and inflow mass flow rates was still around 4 per cent. However, we thought this to be sufficiently close to a quasi equilibrium condition to allow us to evaluate the heat transfer enhancement capabilities of synthetic jets.

*Heat transfer enhancemen*t

The instantaneous local heat flux variation on the hot surface immediately above the centre of the orifice passage at a frequency of 30 kHz is shown in Figure 8 as a function of non-dimensional time from the beginning of the calculations which were started from the steady flow results. There is a is a long transient period, lasting approximately six actuator cycles, before the instantaneous heat transfer rate as a function of time can be said to repeat during an actuator cycle. At all frequencies, the results presented in this section have therefore been selected from the seventh cycle from the beginning of the calculations.

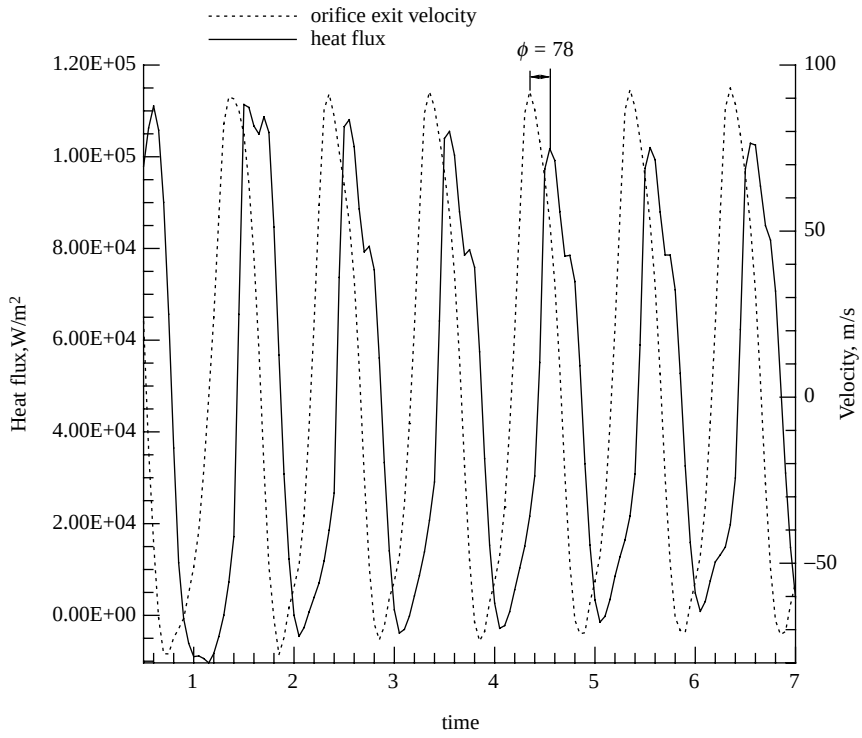

Figure 8.
Vertical velocity at ($x = 0$, $y = 0$) and surface heat flux at ($x = 0$, $y = 200\ \mu$m), $f = 30$ kHz

The heat flux fluctuations as a function of time are rather large; varying from a maximum of 103 kWm^{-2}, which is about 13 times larger the steady flow heat transfer flux at the same location, to a minimum of 6 Wm^{-2}. In fact, the heat flux at the point on the upper wall immediately above the centre of the orifice passage, averaged over the 7th cycle, is 43 kWm^{-2}, which is approximately 5.6 times the steady flow heat flux. Clearly, there has been a very large enhancement in the heat transfer rate at this location.

In fact, as may be seen from Figure 9, the maximum heat flux does not occur at the point immediately above the centre of the orifice, but, depending on the frequency can occur on either side of it. Further, it is interesting to note by comparing Figure 9(a), (b) and (c) that the non-dimensional time at which the maximum heat flux occurs is also dependent on the frequency.

Heat flux distributions as a function of time

As may be shown in Figure 8, there is a significant time-lag between the centreline velocity of the jet at the exit of the orifice and the heat flux on the hot wall. This is obviously due to the time taken by the jet, which starts with a zero velocity at the beginning of the ejection phase of the actuator cycle and gradually increases to a maximum. The time-lag at 30 kHz when expressed as a phase angle is approximately 78°.

Since, the height of the channel was the same in all the cases considered here, the actual time required for the jet to reach the upper wall would inversely proportional to

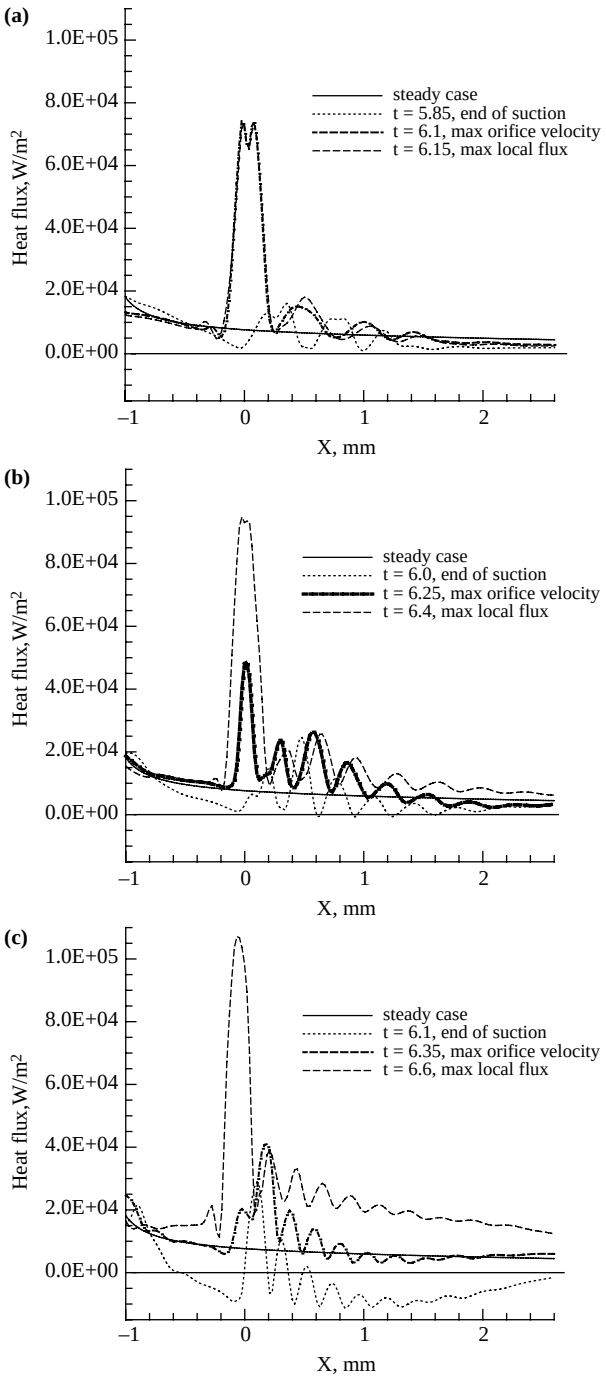

Figure 9.
Local heat flux at different time instants of the cycle, (a) $f = 10$ kHz $A = 40\mu$m; (b) $f = 20$ kHz $A = 20\mu$m; (c) $f = 30$ kHz $A = 40\,\mu$m

the maximum jet velocity at the exit of the orifice. Since, the phase angle is directly proportional to the ratio of the actual time taken to reach the upper wall to the period of the actuator cycle, it follows that the phase angle ϕ_{f_2} at a frequency f_2 would be given by:

$$\phi_{f_2} = \frac{f_2}{f_1} \frac{v_{j_1}}{v_{j_2}} \phi_{f_1} \tag{29}$$

in which the phase angle ϕ_{f_1} is known at a frequency f_1 and v_{j_1} and v_{j_2} are the maximum velocities at the jet exit at the two frequencies.

Although a reasonable effort was expended to obtain a constant value of the maximum jet exit velocity at all frequencies, because of the long transient and the unknown form of $K_1(f)$ in equation (25), it was very difficult to adjust the amplitude of the diaphragm to ensure that this condition was met in all cases. As a result, the value of the maximum velocity at the exit from the orifice varied from a high of 104 ms^{-1} at 10 kHz to a low of 89 ms^{-1} at 20 kHz. Since, the aim of the research was to determine whether synthetic jet actuators are appropriate for enhancing heat transfer in micro-channels carrying air, a 17 per cent changes in the maximum velocity of the jet would not affect the evaluation of the performance of the device.

When the values at 10 and 20 kHz are substituted in equation (29), phase lags of 23 and 50°, respectively, are obtained. These values are in remarkably close agreement with 22 and 50°, respectively, extracted from the numerical calculations. The phase shift due to the time taken for the jet to reach the upper surface has to be added to the phase shift due to compressibility effects discussed earlier, in order to obtain the phase shift relative to the diaphragm motion. Since, the non-dimensional time is based on the movement of the membrane of the actuator, the maximum heat flux must occur at different non-dimensional times at the various frequencies shown in Figure 9. Similarly, different phase shifts occur at different frequencies for other events, such at the time of the end of suction, and need to be taken into account if a consistent set of results for the spatial distribution of the heat flux is to be presented.

Spatial heat transfer distribution

At 10 kHz at the time of the maximum heat transfer rate, there appears to be two maxima of the heat flux occur, one on either side of the orifice, whereas at the other two frequencies there was only one maximum (Figure 9). A stagnation region was detected immediately opposite the orifice at 10 kHz. Interestingly, as the frequency is increased the location of the point at which the maximum local heat flux occurs moves towards the inlet of the main channel, as is clearly shown in the three cases in Figure 9. Further, the horizontal extent of the large maximum heat flux spike depends on the frequency, changing from a maximum of 0.43 mm at 10 kHz to a minimum of 0.29 mm at 30 kHz.

Whilst at the time of maximum heat flux the distributions of the local heat flux appear to be similar, there are significant differences which are due to the frequency at which the actuator is operating. Since, the duration of the ejection phase of the actuator cycle is inversely proportional to the frequency and the average velocity in the channel reduces as the frequency increases, the spacing between adjacent vortices downstream of the orifice will, per force, be reduced as may be seen in Figure 9 from the distances between successive maxima of the heat flux distribution. However, it is not apparent

as to why the increased heat flux spreads further downstream as the frequency becomes larger, as is readily noticeable from a comparison of Figure 9(a) with Figure 9(c).

Because of the lack of mixing at the low frequency of 10 kHz (Figure 9(a)) the heat flux towards the exit falls below the heat flux in the same area when steady flow prevails. Whereas, as can be seen at $t = 6.15$, in the region downstream of the large spike, the heat flux is higher than that obtained in steady flow. At 20 kHz, however, because of the increased mixing, the heat flux, in the region near the exit, is higher than that obtained in steady flow at the time of its maximum. In fact, the heat flux at $t = 6.4$ is significantly higher at all points downstream of the beginning of the large heat transfer spike, than at 10 kHz and that in steady flow (Figure 9(b)). The heat flux at $t = 6.6$ at a frequency of 30 kHz (Figure 9(c)) is very much larger in the region downstream of the large spike than at 20 kHz and very much larger than the steady flow heat flux.

Upstream of the large spike the heat flux at 10 kHz at $t = 6.15$ is slightly lower than the heat flux which prevails at steady flow (Figure 9(a)). At 20 kHz at the time of the maximum heat flux, $t = 6.4$, Figure 9(b), the heat flux upstream of the large spike is approximately the same as that in steady flow, that is slightly higher that that at 10 kHz at the same point in the cycle. As was the case downstream of the large spike at 30 kHz, with $t = 6.6$, the heat flux upstream of the spike is larger than at 10 and 20 kHz and larger than that which obtains in steady flow. Thus, it may be concluded, that in the range of frequencies investigated, at the maximum heat transfer stage of the cycle, the heat transfer rate increases with the frequency.

As may be seen in Figure 9, the time when the maximum jet velocity occurs at the orifice the form of spatial distribution of the instantaneous local heat flux for all frequencies, is similar to that which occurs at the time of the maximum heat flux, but, with the heat flux significantly lower than that which pertains at the later time.

The lowest heat transfer occurs at the end of the suction phase. At 10 kHz, despite there being some regions in which the heat flux is larger that that obtained in steady flow, most of the upper surface yields a heat flux lower than the steady flow heat flux (Figure 9(a)). Similar remarks apply to the heat flux at 20 kHz (Figure 9(b)), which is even lower than at 10 kHz. The results at a frequency of 30 kHz are totally unexpected as may be seen in Figure 9(c). Here the heat flux is very low, with only two small regions in which the heat flux exceeds the heat transfer rate in steady flow. What is remarkable, and therefore totally unexpected, is that downstream of $x \approx 0.4$mm the heat flux is negative, that is, the heat transfer is from the air to the isothermal wall.

In order to be able to transfer heat from the fluid to the wall, the temperature of the fluid in the vicinity of the wall would have to be higher than the temperature of the wall. Since, the hottest boundary is the upper wall, it seems impossible that the fluid could reach a higher temperature. This is indeed true for an incompressible fluid, but is not the case for a compressible fluid. The accelerations in the main channel are a function of the frequency squared, since the velocities are a function of the frequency. As a result the pressure gradients and hence the pressure changes at a particular point in the main channel are also proportional to the frequency squared. That is, during the deceleration phase at 30 kHz, the maximum difference in pressure between the pressure at a point in the main channel, downstream of the orifice, and the external domain, would need to be about 2(1/4) times that which exists at 20 kHz. This is indeed

the case with the maximum pressure difference being 7.2 kPa at 30 kHz, whereas it is 2.9 kPa at 20 kHz; a ratio of 2.5. An isentropic compression from 100 to 107 kPa would lead to a 2 per cent increase in temperature.

Now, during the suction phase there is little flow in the main channel downstream of the orifice, as may be seen Figure 4(d). In fact flow is directed upstream, particularly near the hot, upper wall. That is the hottest air near the hot wall is forced to move upstream getting further heated. A 2 per cent increase in temperature, mentioned above, with the air initially at 323 K, the hot wall temperature, would lead to a temperature 6.3 K higher than the wall temperature. This would result in a significant heat transfer from the air to the hot wall. Now, since the compression is not isentropic because there is heat transfer, the temperature would not rise as much. In fact, the highest temperature near the wall is 4 K higher than the wall temperature; a temperature rise equal to approximately 2/3 of the isentropic temperature rise predicted above. It follows that the pressure rise during deceleration phase in the main channel, coupled with the fact that air is compressible, is responsible for the apparently anomalous heat transfer from the fluid to the hot wall.

The heating process occurs to a lesser extent at 20 kHz, so that there are no regions of negative heat transfer as may be shown in Figure 9(b) at $t = 6.0$. The effect is even smaller at 10 kHz so that the heat transfer at the end of suction, is not much less than the steady state heat transfer. As is shown in Figure 9, the much larger changes in pressure at 30 kHz are therefore responsible for the very bigger fluctuations in the heat flux in time than those at 10 or 20 kHz.

Work is required to increase the pressure and temperature in the main channel and this is supplied by work, additional to that which would be provided by the diaphragm, if the actuator were operating in a still ambient atmosphere. The magnitude of the extra work, and its consequences in evaluating the viability of using synthetic jet actuators, has not been determined because, at this stage the effectiveness of the synthetic jet as a means of heat transfer enhancement is to be established.

Overall heat transfer rates

There is a significant increase in the overall heat transfer averaged over the whole length of the channel and over an actuator cycle as is shown in Figure 10. The heat flux shown by the lower curve in Figure 10 increases as the frequency becomes larger. This is despite the fact that at 30 kHz there is a heat transfer from the air to the hot wall for part of the cycle, which does not happen at the lower frequencies. The heat flux at 30 kHz is 37 per cent larger than the heat flux obtained when the flow is steady. However, the increase in heat flux when the frequency is changed from 10 to 30 kHz is only 18 per cent. It is interesting to note that the heat flux increase has occurred despite a 19 per cent reduction in the inlet air velocity as the frequency is increased from zero to 30 kHz.

It may be seen in Figure 9 that the effect of the synthetic jet diminishes beyond $x = 2$ mm so that it is more appropriate to evaluate the effect of the jet over the region from the entrance $x = -1.1$ mm, to $x = 2$ mm. The upper curve in Figure 10 shows the heat flux averaged over this region and over one cycle of the membrane motion. Here, the enhancement in the average flux is somewhat larger then when the heat flux is averaged over the whole length of the channel, being 42 per cent. Interestingly, the gradient of the upper line in Figure 10 is smaller than the lower curve. This means that

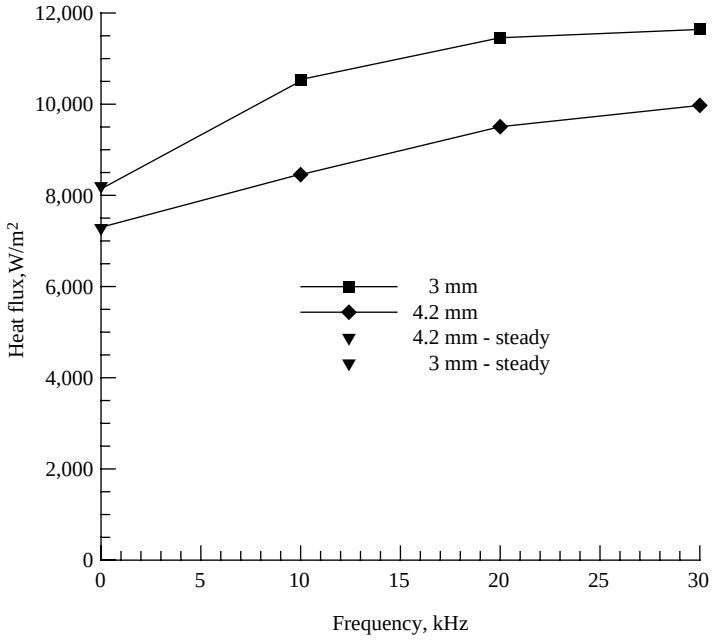

Figure 10.
Time and surface averaged heat flux for different frequencies

the enhancement in the heat flux smaller when the frequency is increased for 10-30 kHz, when the heat flux is averaged over the shorter region. This is in agreement with the fact, mentioned above, that as the frequency is increased, the effect of the mixing seems to affect the heat transfer further downstream.

In any case, the heat transfer rates which need to be handled in microchips have to be orders of magnitude higher that the maximum heat flux averaged over time and space of about $11\,\mathrm{kWm}^{-2}$ obtained in this study, so that it seems unlikely that synthetic jets can provide sufficient heat enhancement to make air cooled micro-channels a viable method of heat removal in future generations of microchips.

Conclusions

A model has been developed of the flow and heat transfer processes in forced convection an air cooled micro-channel with an isothermal hot wall and in which a synthetic jet was used to enhance the heat transfer. Here, the compressibility effects of the air were included and the motion of the diaphragm of the actuator was directly simulated.

It was demonstrated that compressibility of air is very significant and a simple method was found for determining the natural frequency of the cavity as well as allowing a reasonable estimates of the phase angle between the velocity of the air at the exit from the orifice of the actuator and the diaphragm motion, once a reliable value of the damping could be established.

Once the actuator was switched on, a flow pattern consisting of geared vortices occurred downstream of the jet during the ejection phase of the actuator cycle. Surprisingly, the vortices persisted during the ingestion part of the cycle. The distance

between adjacent vortices decreased as the frequency increased. Upstream of the orifice, large fluctuations in velocity occurred, including flow reversals.

As expected, the heat flux results as a function of time, at a point on the hot wall immediately above the orifice, lag in the air velocity at the exit of the. At that point on the hot wall, and adjacent points, there are very large fluctuations in the heat transfer flux which increase with the frequency, however, on the average, there is a very significant enhancement of the heat transfer from its value in steady flow, for example at 30 kHz the average heat transfer flux in this area is 5.6 times the steady flow value. Although superficially the same, at the time of maximum heat transfer, the better mixing which results from the larger density of vortices as the frequency increases results in larger heat fluxes downstream of the orifice.

An apparent anomaly occurs at the beginning of the ejection cycle at 30 kHz down stream of the orifice. At that time, in the majority of the channel, there is heat transfer from the "cooling" air to the "hot" isothermal surface. The large accelerations required to adjust fluid velocities at 30 kHz, result in pressure changes, which, because of the compressibility of air, are sufficiently large to increase the temperature of the air near the isothermal boundary to above that of the wall, leading to heat transfer from the fluid to the wall. It is seen here that if air is used for cooling in situations in which large pressure changes may occur, this may lead to a significant decrease, or even a reversal, as occurs at 30 kHz, of heat transfer.

Despite the reversal of heat transfer at some points during part of the actuator cycle, the heat flux averaged over time and space, increases as the frequency increases. The enhancement is, however, only 37 per cent over that obtained in steady flow. Since, the heat fluxes required in the next generation of microchips are orders of magnitude larger than those found in this study, it seems unlikely that air forced convection in micro-channels will lead to viable devices, even if the cooling is enhanced by synthetic jets.

References

Eroglu, A. and Breidenthal, R.E. (2001), "Structure, penetration, and mixing of pulsed jets in crossflow", *AIAA Journal*, Vol. 39 No. 3, pp. 417-23.

Glezer, A. and Amitay, M. (2002), "Synthetic jets", *Ann. Rev. Fluid Mech.*, Vol. 34, pp. 503-29.

Gordon, M. and Soria, J. (2001), "Scalar mixing of zero-net-mass-flux jets in crossflow", *Proc. 14th Australasian Fluid Mech. Conf.*, pp. 729-32.

Ho, C.M. and Huang, L.S. (1982), "Subharmonics and vortex merging in mixing layers", *J. Fluid Mech.*, Vol. 119, pp. 443-73.

Karniadakis, G. and Beskok, A. (2002), *Micro Flows: Fundamentals and Simulation*, Springer-Verlag Inc., New York, NY.

Kataoka, K., Suguro, M., Degawa, H., Maruo, K. and Mihata, I. (1987), "The effect of surface renewal due to large scale eddies on jet impingement heat transfer", *Int. J. Heat Mass Transfer*, Vol. 30, pp. 559-67.

Kreyszig, E. (1972), *Advanced Engineering Mathematics*, Wiley, New York, NY.

Mallinson, S.G., Kwok, C.Y. and Reizes, J.A. (2003), "Numerical simulation of micro-fabricated zero mass-flux jet actuators", *Sensors and Actuators A*, Vol. 105, pp. 229-36.

Mladin, E. and Zumbrunnen, D. (2000), "Alterations to coherent flow structures and heat transfer due to pulsations in an impinging air-jet", *Int. J. Term.Sci.*, Vol. 39, pp. 236-48.

Smith, B.L. and Glezer, A. (1998), "The formation and evolution of synthetic jets", *Physics Fluids*, Vol. 10 No. 9, pp. 2281-97.

Timchenko, V., Reizes, J. and Leonardi, E. (2004), "Compressibility effects in micro synthetic jets", paper presented at 2nd Int. Conference on Microchannels and Minichannels, Rochester, New York, 17-19 June, Paper 32-1D.

Tuckerman, D.B. and Pease, R.F.W. (1981), "High performance heat sinking for VLSI", *IEEE Electron Device Letters*, Vol. EDL-2 No. 5, pp. 126-9.

Corresponding author
Victoria Timchenko can be contacted at: v.timchenko@unsw.edu.au